Numerical simulation of high strength circular double-skin concrete-filled steel tubular slender columns

Liang, Q. Q. (2018). Numerical simulation of high strength circular double-skin concrete-filled steel tubular slender columns. *Engineering Structures*, 168: 205-217.

Numerical simulation of high strength circular double-skin concrete-filled steel tubular slender columns

Qing Quan Liang *

College of Engineering and Science, Victoria University, PO Box 14428, Melbourne, VIC 8001, Australia

ABSTRACT

Circular double-skin concrete-filled steel tubular (DCFST) slender columns made of high-strength concrete are high performance structural members with wide applications in engineering structures. However, research studies on the behavior, load distributions in concrete and steel components and confinement characteristics of such composite columns under eccentric loading have been very limited. This paper describes a new mathematical model that computes the axial load-deflection performance of high-strength circular DCFST slender columns subjected to eccentric loading. The incremental nonlinear equilibrium equations of DCFST slender columns are solved by the developed efficient computational procedure and numerical solution algorithms accounting for initial geometric imperfections and second order effects. The mathematical model incorporates the accurate material constitutive laws of sandwiched concrete, which accurately predict the residual concrete strength and strain in the post-yield regime. The computer program implementing the mathematical model is utilized to quantify the influences of geometric and material properties and concrete confinements on the load-deflection behavior, column strength curves and load distributions in circular DCFST slender columns. It is shown that the mathematical model not only accurately predicts the experimental behavior of circular DCFST slender columns but

* Corresponding author. Tel.: +61 3 9919 4134.
E-mail address: Qing.Liang@vu.edu.au (Q. Q. Liang)

also effectively monitors the load distributions in concrete and steel components of DCFST slender columns under deflection increments. The proposed mathematical model is an accurate and efficient computational and design technique for circular DCFST slender columns.

Keywords: Concrete-filled steel tubes; Double-skin; High-strength concrete; Nonlinear analysis; Slender composite columns.

1. Introduction

The inner steel tube in a circular DCFST slender column as depicted in Fig. 1 is not filled with concrete, which results in not only a reduction in its weight but also an increase in its stiffness-to-weight ratio, ductility and seismic resistance. However, the ultimate axial strength of the circular DCFST slender column may be lower than that of the concrete-filled steel tubular (CFST) column for the concrete usually shares a large part of the column ultimate axial load. To increase the ultimate axial loads of DCFST columns, high-strength concrete can be utilized to fill the double-skin steel tubes. This leads to high performance DCFST columns. However, only very limited experiments on circular DCFST slender columns have been conducted, such as those by Tao et al. [1], Essopjee and Dundu [2] and Ibañez et al. [3], and no numerical studies on high-strength DCFST slender columns made of carbon steel tubes have been undertaken. Moreover, there is a lack of understanding of the load distributions and concrete confinement characteristics in circular DCFST slender columns. Therefore, an efficient and accurate numerical simulation tool is much needed for investigating the performance, confinement characteristics and load distributions in steel tubes and concrete of DCFST slender columns.

Tests on circular CFST columns were undertaken by Knowles and Park [4], Neogi et al. [5], Rangan and Joce [6], Schneider [7], Giakoumelis and Lam [8] and Portolés et al. [9]. Test results indicated that the performance of the filled concrete in terms of strength and ductility in circular CFST columns with relatively small column slenderness ratios was improved because the circular steel tube confined the concrete infill. Knowles and Park [4] proposed limiting column slenderness for concentrically-loaded CFST circular columns in which the confinement effect should be considered in the design. Liang [10, 11] reported that the confinement in circular CFST columns was a function of the tube diameter-to-thickness ratio, eccentricity of applied load and column slenderness. Test results showed that both the inner and outer circular tubes provided confinement to the sandwiched concrete in a DCFST short column, as provided by Tao et al. [1], Wei et al. [12], Zhao et al. [13], Han et al. [14] and Uenaka et al. [15]. However, no investigations have been undertaken on the confinement characteristics of circular DCFST slender columns constructed by carbon steel tubes.

Limited experiments on circular DCFST slender columns subjected to eccentric loading or axial compression were performed in the past [1-3]. Tao et al. [1] tested twelves pin-ended circular DCFST slender columns where the column slenderness ratios (L/r) varying from 28.3 to 56.5, loading eccentric ratios (e/D_o) ranging from 0.0 to 0.395 and inner-to-outer tube-diameter ratio (D_i/D_o) of 0.509. The experimental results showed that these DCFST slender columns failed by global buckling without any tube local buckling. It was found that the ultimate axial load as well as the flexural stiffness of DCFST slender columns decreased with an increases in the L/r ratio or e/D_o ratio. Specimens with a larger e/D_o ratio exhibited better ductility. Essopjee and Dundu [2] carried out experiments on 32 pin-ended circular DCFST slender columns under axial compression with slenderness ratios (L/r) ranging from 25 to 63.9, the D_o/t_o ratios varying from 46.4 to 55, and D_i/t_i ratio of 38. The failure modes

associated with the columns having an L/r ratio of 25 were the yielding and the outer steel tube local buckling and crushing of the sandwiched concrete while other columns exhibited overall buckling behavior without local buckling. Ibañez et al. [3] conducted tests on four eccentrically-loaded circular DCFST slender columns with normal or ultra-high strength concrete. The parameters examined were D_o / t_o and D_i / t_i ratios and concrete strengths.

Computational models that calculated the nonlinear responses of CFST circular columns were developed by Hajjar et al. [16], Susantha et al. [17], Shanmugam et al. 18], Hu et al. [19], Hatzigeorgiou [20], Liang and Fragomeni [21], Portolés et al. [22], Mollazadeh and Wang [23], Kostic et al. [24], Yang and Han [25] and Schnabl et al. [26]. Hu et al. [19] and Liang and Fragomeni [21] developed confinement models for the concrete confined by circular steel tubes, which can be used in numerical analysis procedures. Simulation techniques considering concrete confinement generally provided more accurate results on the performance of circular CFST columns than those ignoring confinement effects [21]. The strength and behavior of circular DCFST short columns were examined by using computer simulations techniques by Tao et al. [1], Wei et al. [27], Huang et al. [28], Hu and Su [29], Pagoulatou et al. [30], Hassanein et al. [31] and Liang [32]. However, the numerical nonlinear analyses of circular DCFST slender columns subjected to eccentric loading have been rare. The only available numerical investigation on circular DCFST slender columns made of carbon steel tubes was conducted by Tao et al. [1]. The material laws of concrete in circular CFST columns were employed in their fiber model, which ignored the confinement caused by the internal tube. Hassanein and Kharoob [33] used the commercial finite element software ABAQUS to study the behavior of circular double-skin concrete-filled tubular slender columns with external stainless steel tubes. They applied the confinement model proposed by Liang and Fragomeni [21] for concrete in CFST columns to the sandwiched concrete in DCFST columns, and did

not considered the confinement effect provided by the inner steel tube. Experimental results showed that the stress-strain behavior of stainless steel in compression is significantly different from that in tension [34]. However, the stress-strain laws for stainless steel used by Hassanein and Kharoob [33] in their finite element models did not account for the different strain-hardening characteristics of stainless steel in compression and tension. The confinement effect on the behavior of double-skin concrete-filled tubular slender columns with external stainless steel tubes was investigated. Ky et al. [35] reported on a fiber element model that predicted the inelastic behavior of axially-loaded concrete encased composite short and slender columns considering concrete confinement, the buckling of steel sections and reinforcing bars and initial geometric imperfections.

The confinement effect on the filled concrete in a circular DCFST column is significantly different from that on concrete core in a circular CFST column. Hu and Su [29] proposed a constitutive model for determining the lateral pressures on the concrete sandwiched by both steel tubes in circular DCFST columns. Pagoulatou et al. [30] utilized the confinement model given by Hu and Su [29] in the finite element analysis of DCFST short columns. Liang [32] proposed accurate material constitutive laws for quantifying the post-peak strength and strain of sandwiched concrete confined by circular tubes. The fiber-based technique developed by Liang [32] was found to accurately quantify the experimentally observed behavior of short circular DCFST columns. The load distributions in concrete and steel components of circular DCFST short columns have been investigated by Huang et al. [28] and Liang [32], which gave a better understanding of the load distribution mechanism in DCFST short columns. However, no investigations have been performed on the load distributions in circular DCFST slender columns subjected to eccentric loading.

This paper concerns with the computational simulations of the behavior of eccentrically-loaded circular slender DCFST columns constructed by high-strength concrete for the first time. A new mathematical model is developed to calculate the axial load-deflection responses of circular DCFST slender columns considering geometric and material nonlinearities. The mathematical formulations and computational algorithms that solve the inelastic stability problem of DCFST slender columns are described. The accurate constitutive laws of sandwiched concrete and structural steels considering concrete confinement are presented. The experimental results published are used to verify the mathematical model. A parametric study is given that examines the influences of various geometric and material properties on the load-deflection behavior, column strength curves, load distributions and confinement characteristics of high-strength DCFST slender columns.

2. Mathematical model for DCFST slender columns

2.1. Assumptions

The following assumptions are made in the mathematical formulations of the model:

(1) The bond between the sandwiched concrete and the outer and inner steel tubes is perfect;

(2) Plane sections remain plan after deformation, which results in a linear distribution of strains through the depth of the cross-section as depicted in Fig. 2;

(3) The confinement effect provided both outer and inner steel tubes is considered by using the stress-strain laws for confined concrete;

(4) The local buckling of circular steel tubes is not taken into account;

(5) Failure occurs when the concrete strain of the extreme compression fiber attains the maximum strain;

(6) The effect of concrete creep and shrinkage is ignored.

2.2. Modeling of cross-sections

The mathematical model utilizes the fiber element method to discretize the cross-section of a circular DCFST slender column as discussed by Liang [36-38] and Patel et al. [39]. Figure 2 illustrates a typical mesh of fibers. Different material properties can be assigned to the fibers of the two steel tubes while concrete properties are assigned to the fibers of sandwiched concrete. Stresses in fibers are computed from corresponding strains using the uniaxial material constitutive laws presented in Section 3. The fiber strains are determined from the depth of neutral axis (d_n) and curvature (ϕ) of the cross-section subjected to eccentric loading as depicted in Fig. 2 [36]. The axial force and moment are calculated by

$$P = \sum_{j=1}^{nso} \sigma_{so,j} A_{so,j} + \sum_{k=1}^{nsi} \sigma_{si,k} A_{si,k} + \sum_{n=1}^{nc} \sigma_{c,n} A_{c,n} \tag{1}$$

$$M = \sum_{j=1}^{nso} \sigma_{so,j} A_{so,j} y_j + \sum_{k=1}^{nsi} \sigma_{si,k} A_{si,k} y_k + \sum_{n=1}^{nc} \sigma_{c,n} A_{c,n} y_n \tag{2}$$

in which P represents the axial force; M stands for the section moment about the x axis; subscripts j, k and n represent the fibers in the external steel tube, internal steel tube and sandwiched concrete, respectively; subscripts *so*, *si* and *c* stand for external tube, internal tube and sandwiched concrete respectively; σ, A and y are the longitudinal stress, area and coordinate of the fiber respectively; *nso*, *nsi* and *nc* are the total numbers of fiber elements in the external tube, internal tube and sandwiched concrete, respectively.

2.3. Modeling of axial load-deflection responses

A mathematical model is developed for pin-ended DCFST slender columns under eccentric loading with an equal eccentricity at both ends and bending into single curvature as schematically depicted in Fig. 3. The initial geometric imperfection of the slender column and second-order effects caused by the applied load and deflections are included in the formulation [10]. The part-sine displacement function is employed to describe the deflected shape of circular DCFST slender columns. As discussed by Liang [10], the curvature at the column mid-height is derived from the displacement function as

$$\phi_m = u_m\left(\frac{\pi}{L}\right)^2 \tag{3}$$

The moment induced by the external applied load at the column mid-height is determined as

$$M_e = P\left(e + u_{\mathrm{o}} + u_m\right) \tag{4}$$

where P is the applied axial load as shown in Fig. 3, e is the loading eccentricity, u_{o} represents the initial out-of-straightness at the column mid-height, and u_m is the deflection at the column mid-height.

The geometric and material nonlinear analysis requires that the moment equilibrium at the mid-height of the slender DCFST columns under eccentric loading must be satisfied. This condition is expressed by

$$P\left(e+u_{\mathrm{o}}+u_m\right)-M_i=0 \tag{5}$$

In the numerical analysis, if the absolute value of the residual moment $\rho_m=P\left(e+u_{\mathrm{o}}+u_m\right)-M_i$ is less than the convergence tolerance, such as $\left|\rho_m\right|<\varepsilon_k$, the equilibrium condition is satisfied.

An incremental and iterative process is proposed to compute the applied axial load from a given deflection increment at the column mid-height. The displacement control method is implemented in the nonlinear analysis. The internal axial force (P) and bending moment (M_i) are computed for a given mid-height deflection. The internal axial force satisfying the equilibrium condition is treated as the axial load applied at the column ends. This analysis process is repeated to capture the complete axial load-deflection curve [10, 11].

The computational procedure is developed to compute the axial loads from given deflections of circular DCFST slender columns:

1. The initial geometric imperfection, geometries, material properties and loading eccentricity of the DCFST slender column are specified.
2. The steel tubes and sandwiched concrete are discretized into layers by specifying the numbers of layers respectively. The sizes of concrete and steel fibers in the circular direction are automatically calculated based on the thickness of layers as illustrated in Fig. 2. Based on the mesh, the coordinates and areas of fiber elements are computed and stored.
3. The deflection at the column mid-height is initialized as $u_m=\Delta u_m$.
4. The column mid-height curvature (ϕ_m) is computed using Eq. (3).

5. The initial values are assigned to three neutral axis depths of the cross-section as follows: $d_{n1} = D/4$, $d_{n2} = D/2$, $d_{n2} = D$.

6. The constitutive laws of steel and sandwiched concrete given in Section 3 are used to compute stresses in fibers from strains.

7. The internal axial force P and moment M_i are calculated from fiber stresses.

8. Three residual moments (ρ_{m1}, ρ_{m2}, ρ_{m3}) are computed from three initial neutral axis depths (d_{n1}, d_{n2}, d_{n3}).

9. The neutral axis depth (d_{n4}) is calculated using Müller's numerical scheme [40] in order to determine the true d_n.

10. Material constitutive laws are employed to compute stresses in fibers from strains.

11. The internal axial force P and moment M_i are computed from stresses as stress resultants.

12. Repeat Steps (9) to (11) until the residual moment ρ_{m4} computed using d_{n4} is less than the specified convergence tolerance, such as $|\rho_{m4}| < 10^{-4}$. The internal axial force P so determined is equal to the applied axial load for the deflection u_m.

13. The deflection at the column mid-height is increased as follows: $u_m = u_m + \Delta u_m$.

14. The analysis process is repeated from Steps (4) to (13) until $P < 0.5P_{\max}$ or the specified limit on deflection is exceeded. The maximum axial load $P_{\max}$ recorded in the analysis is determined as the ultimate axial strength (P_u) of the slender DCFST column.

In the nonlinear analysis of real DCFST slender columns with initial geometric imperfections, the load-deflection curve obtained is nonlinear. The ultimate axial load predicted by the numerical model is the buckling load of the real DCFST slender column. The computational

procedure proposed can be used to calculate the buckling loads/ultimate loads of DCFST slender columns under axial compression without initial geometric imperfections or incorporating a very small initial geometric imperfection.

2.4. Numerical solution algorithms

Computational algorithms implementing Müller's method [40] is developed to iteratively adjust the depth of neutral axis (d_n) in the cross-section of the DCFST column to calculate the internal force from the moment equilibrium condition as reported by Patel et al. [41] and Liang et al. [42]. The method starts with three estimates of the neutral axis depths d_{n1}, d_{n2} and d_{n3}. The next estimate of the depth of neutral axis (d_{n4}) is calculated by the following expressions and the process is repeated until the true neutral axis depth is obtained:

$$d_{n4} = d_{n3} - \frac{2C}{B \pm \sqrt{B^2 - 4AC}} \tag{6}$$

$$A = \frac{(\rho_{m1} - \rho_{m3})(d_{n2} - d_{n3}) - (\rho_{m2} - \rho_{m3})(d_{n1} - d_{n3})}{(d_{n1} - d_{n2})(d_{n1} - d_{n3})(d_{n2} - d_{n3})} \tag{7}$$

$$B = \frac{(\rho_{m2} - \rho_{m3})(d_{n1} - d_{n3})^2 - (\rho_{m1} - \rho_{m3})(d_{n2} - d_{n3})^2}{(d_{n1} - d_{n2})(d_{n1} - d_{n3})(d_{n2} - d_{n3})} \tag{8}$$

$$C = \rho_{m3} \tag{9}$$

where both signs of B and the square root term in the denominator are the same. The values of d_{n1}, d_{n2} and d_{n3} are exchanged in order to obtain the true neutral axis depth [41, 42].

2.5. Contribution ratios of concrete and steel tubes

The contributions of concrete and steel tubes to the ultimate axial load of a circular DCFST slender column are quantified using contribution ratios, which can be utilized to study the economical designs of slender DCFST columns. The contribution ratios are defined as

$$R_{so} = \frac{P_{u.so}}{P_u} \tag{10}$$

$$R_{si} = \frac{P_{u.si}}{P_u} \tag{11}$$

$$R_c = \frac{P_{u.c}}{P_u} \tag{12}$$

where R_{so}, R_{si} and R_c are the contribution ratios of the external steel tube, internal steel tube and sandwiched concrete, respectively; $P_{u.so}$, $P_{u.si}$ and $P_{u.c}$ are the axial loads carried by the external tube, internal tube and sandwiched concrete when the DCFST column attains its ultimate strength, respectively. These axial loads and the ultimate axial strength (P_u) of a slender circular DCFST column are computed using the axial load-deflection analysis procedure described previously.

3. Constitutive laws of sandwiched concrete

3.1. Idealized stress-strain curve of sandwiched concrete

The idealized stress-strain curves for confined sandwiched concrete and unconfined concrete subjected to compression and tension are depicted in Fig. 4 [10, 11]. For concrete in

compression, the ascending branch OA describes the pre-peak behavior while the linearly descending branch AB and the constant branch BC represent the post-peak behavior. The confinement exerted by the steel tubes to the sandwiched concrete is considered in the constitutive laws of sandwiched concrete, which are given in the following sections.

3.2. Compressive strength and strain of confined concrete

The sandwiched concrete in a circular DCFST column under applied loads is subjected to lateral pressures (f_{rp}) provided by the external and internal steel tubes. This lateral pressure needs to be determined to quantify the compressive strength ($f_{cc}^{'}$) and corresponding strain ($\varepsilon_{cc}^{'}$) of the confined sandwiched concrete [10, 11]. In the present mathematical model, empirical equations given by Richart et al. [43] and Mander et al. [44] and modified by Liang and Fragomeni [21] with the factor γ_c are employed to calculate the maximum compressive strength and corresponding strain of sandwiched concrete as follows:

$$f_{cc}^{'} = \gamma_c f_c^{'} + k_1 f_{rp} \tag{13}$$

$$\varepsilon_{cc}^{'} = \left(1 + \frac{k_2 f_{rp}}{\gamma_c f_c^{'}}\right)\varepsilon_c^{'} \tag{14}$$

in which $k_1 = 4.1$ and $k_2 = 20.5$ are constant coefficients obtained from experiments reported by Richart et al. [43], and γ_c was given by Liang [36] to incorporate the effect of column sizes, which is determined by

$$\gamma_c = 1.85 D_c^{-0.135} \quad (0.85 \le \gamma_c \le 1.0) \tag{15}$$

in which D_c is calculated by $D_c = D_o / 2 - t_o - D_i / 2$ for sandwiched concrete.

The strain $\varepsilon_c^{'}$ corresponding to $f_c^{'}$ of the unconfined concrete varies from 0.002 to 0.003 depending on the effective compressive strength ($\gamma_c f_c^{'}$) of concrete [36].

Hu and Su [29] studied the test results of circular DCFST columns given by Tao et al. [1] and proposed expressions for computing the lateral pressures on concrete in circular DCFST columns considering the confinement caused by the external and internal steel tubes. Liang [32] has evaluated the validity of the expressions for lateral pressures given by Hu and Su [29] and recommended the following formula be used to estimate the lateral pressure:

$$f_{rp} = 8.525 - 0.166\left(\frac{D_o}{t_o}\right) - 8.97\times10^{-3}\left(\frac{D_i}{t_i}\right) + 1.25\times10^{-3}\left(\frac{D_o}{t_o}\right)^2 + 2.46\times10^{-3}\left(\frac{D_o}{t_o}\right)\left(\frac{D_i}{t_i}\right) - 5.5\times10^{-3}\left(\frac{D_i}{t_i}\right)^2 \geq 0 \quad (16)$$

Eq. (16) was developed on the basis of test results on circular DCFST columns with $20 \leq D_o / t_o \leq 100$ and $15 \leq D_i / t_i \leq 55$ as discussed by Liang [32]. Therefore, it can be used to estimate the lateral pressures on sandwiched concrete in DCFST columns within the limiting diameter-to-thickness ratios.

It should be noted that the loading eccentricity causes bending moments and the linear distribution of the strain through the depth of the cross-section as depicted in Fig. 2. The concrete fibers above the neutral axis are in compression while the concrete fibers below the neutral axis are in tension. The confinement model represented by Eqs. (13) and (14) is used

to determine the maximum compressive strength ($f_{cc}^{'}$) of concrete and corresponding strain ($\varepsilon_{cc}^{'}$) due to the confinement effect. As indicated in Eq. (13) and shown in Fig. 4, the confinement effect is considered when the compressive stress in the concrete fibers is greater than $\gamma_c f_c^{'}$. When the compressive stress in the concrete fibers is greater than $\gamma_c f_c^{'}$ and less than $f_{cc}^{'}$, the confinement provided by the steel tubes is between zero and maximum value. As the compressive stresses of concrete fibers vary with the depth of the cross-section, the confinement/lateral pressure also varies with the section depth. This means that the confinement to the concrete fibers is non-uniform. The non-uniform distribution of concrete confinement within the cross-section is approximately simulated by using the stress-strain relationships for confined concrete considering a non-uniform strain distribution.

3.3. Pre-peak behavior of concrete in compression

The branch OA of the stress-strain curve illustrated in Fig. 4 is determined by the expression of Mander et al. [44] as follows:

$$\sigma_c = \frac{\left(\lambda f_{cc}^{'}\right)\left(\varepsilon_c / \varepsilon_{cc}^{'}\right)}{\left(\varepsilon_c / \varepsilon_{cc}^{'}\right)^{\lambda} + \lambda - 1} \tag{17}$$

$$\lambda = \frac{E_c}{E_c - \left(f_{cc}^{'} / \varepsilon_{cc}^{'}\right)} \tag{18}$$

where σ_c stands for the concrete compressive longitudinal stress, and ε_c the longitudinal strain. The Young's modulus (E_c) of concrete is estimated using the formula by the ACI Committee 363 [45] for normal and high strength concrete [36].

3.4. Post-peak behavior of concrete in compression

The post-peak behavior of the sandwiched concrete represented by branches *AB* and *BC* shown in Fig. 4 is expressed by

$$\sigma_c = \begin{cases} \dfrac{\left(f_{cc}^{'} - \beta_c f_{cc}^{'}\right)\left(\varepsilon_{cB} - \varepsilon_c\right)}{\left(\varepsilon_{cB} - \varepsilon_{cc}^{'}\right)} + \beta_c f_{cc}^{'} & \text{for } \varepsilon_{cc}^{'} < \varepsilon_c \le \varepsilon_{cB} \\ \beta_c f_{cc}^{'} & \text{for } \varepsilon_c > \varepsilon_{cB} \end{cases} \tag{19}$$

The post-peak characteristics of the sandwiched concrete are quantified using the strain ε_{cB} and the factor β_c as illustrated in Fig. 4. The values of the strain ε_{cB} and factor β_c determine the degree of confinement offered by the external and internal tubes to the sandwiched concrete. Liang [32] analyzed experimental results on circular DCFST columns reported by Tao et al. [1] and proposed the following expressions for strain ε_{cB}:

$$\varepsilon_{cB} = \begin{cases} 0.03 & \text{for } D_o / t_o \le 60 \\ 0.023 + \dfrac{(100 - D_o / t_o)(0.03 - 0.023)}{(100 - 60)} & \text{for } 60 < D_o / t_o \le 100 \\ 0.02 & \text{for } D_o / t_o > 100 \end{cases} \tag{20}$$

It appears from Eq. (20) that the strain ε_{cB} varies from 0.02 to 0.03 with the D_o / t_o ratio. This reflects the test observations reported by Tao et al. [1]. The linear interpolation method is used to calculate the strain ε_{cB} for sections with D_o / t_o ratios ranging from 60 to 100.

The factor β_c depends not only on the D_o / t_o ratio of the external tube but also on the D_i / t_i ratio of the internal tube. Steel tubes with smaller D_o / t_o and D_i / t_i ratios provide higher

confinement to the sandwiched concrete. By analyzing test results provided by Tao et al. [1] and numerical analyses conducted by Liang [32], Liang [32] proposed the following expressions for the factor β_c that are applicable to the sandwiched concrete confined by circular steel tubes:

$$\beta_c = \begin{cases} 1.0 & \text{for } D_o/t_o \le 40 \\ k_3 & \text{for } D_o/t_o > 40 \\ 3.39\times10^{-5}(D_o/t_o)^2 - 1.0085\times10^{-2}(D_o/t_o) + 1.349 & \text{for } k_3 < 0 \end{cases} \tag{21}$$

where the concrete strength degradation factor k_3 given by Hu and Su [29] is expressed by

$$\begin{aligned} k_3 = {} & 1.73916 - 8.62\times10^{-3}\left(\frac{D_o}{t_o}\right) - 4.731\times10^{-2}\left(\frac{D_i}{t_i}\right) - 3.6\times10^{-4}\left(\frac{D_o}{t_o}\right)^2 \\ & + 1.34\times10^{-3}\left(\frac{D_o}{t_o}\right)\left(\frac{D_i}{t_i}\right) - 5.8\times10^{-4}\left(\frac{D_i}{t_i}\right)^2 \ge 0 \end{aligned} \tag{22}$$

The mathematical model assumes that the internal tube will not undergo local buckling so that it confines the sandwiched concrete. Liang [9, 10] suggested that β_c can be taken as 1.0 when the outer steel tube has a D_o/t_o ratio less or equal to 40. Numerical studies conducted by Liang [32] showed that the strength degradation factor k_3 computed using Eq. (22) in some cases is negative. For these cases, the formula proposed by Hu et al. [19] is employed to calculate β_c in Eq. (21). It should be noted that the factor β_c is within the range of $0 \le \beta_c \le 1.0$.

3.5. Sandwiched concrete in tension

The sandwiched concrete in circular DCFST slender columns under eccentric loading may be subjected to tension. The idealized stress-strain curve of sandwiched concrete under tension is depicted in Fig. 4. The figure shows that the stress increases linearly with an increase in the strain up to concrete cracking. After concrete cracking, the stress decreases linearly with increasing the strain to zero. The concrete tensile strength is determined as $0.6\sqrt{\gamma_c f_c^{'}}$. The ultimate tensile strain of concrete is specified as 10 times the strain at cracking in the present mathematical model.

4. Constitutive laws of structural steels

The outer steel tube of a circular DCFST column under compression may be subjected to hoop tension and longitudinal compression while the internal steel tube carries biaxial compression due to the confinement effect as discussed by Liang [30]. The hoop tension or hoop compression reduces the steel yield stress in the longitudinal direction. This effect is considered in the stress-strain relationship of structural steels depicted in Fig. 5. For high-strength steels, a straight line replaces the rounded part of the curve shown in Fig. 5 The rounded part can be determined by the expression developed by Liang [36].

5. Verification of the mathematical model

The results obtained by Tao et al. [1] and Essopiee and Dundu [2] from tests on circular DCFST slender columns are used to verify the proposed mathematical model. The details of the tested circular DCFST slender columns are provided in Table 1. The diameter-to-thickness ratios of all specimens were within the ranges of $20 \le D_o / t_o \le 100$ and $15 \le D_i / t_i \le 55$. The strength of concrete cylinder ($f_c^{'}$) was calculated by multiplying that of the concrete cube

with a factor of 0.85. In the numerical analyses, the tensile strengths of the external and internal steel tubes of specimens tested by Tao et al. [1] were assumed to be 430 and 450 MPa, respectively. The initial out-of-straightness of all specimens were not measured in the tests. However, the numerical analyses accounted for an initial out-of-straightness of $L/1000$ at the column mid-height, except relatively short columns with one meter long tested by Essopiee and Dundu [2] and Specimens S193.7-1.5a and S193.7-1.5b.

The calculated ultimate axial strengths ($P_{u.\mathrm{num}}$) and experimental ones ($P_{u.\mathrm{exp}}$) of circular DCFST slender columns is given in Table 1. The comparison demonstrates that numerical solutions agree well with experimental data. The statistical analysis on the results of 44 DCFST slender columns indicates that the mean ratio of $P_{u.\mathrm{num}}/P_{u.\mathrm{exp}}$ is 0.997, the standard deviation of $P_{u.\mathrm{num}}/P_{u.\mathrm{exp}}$ is 0.05 and its coefficient of variation is 0.051. The 44 circular DCFST slender columns tested and analyzed cover a wide range of geometric and material properties and loading eccentricities. It is shown that the mathematical model developed is an accurate predictor of the strengths of slender circular DCFST columns under axial loading or eccentric loading.

Fig. 6 presents the computational and experimental axial loads of slender DCFST columns tested by Tao et al. [1] as a function of deflections. The figure illustrates that the measured axial load-deflection responses of DCFST slender columns are generally well captured by the computer programs. In addition, the computed initial flexural stiffness is in closed agreement with the measured one. Moreover, the proposed simulation technique generally predicts well the post-peak characteristics of these DCFST columns. However, it is observed that a slight difference between the predicted and measured axial load-deflection curves exists. This is caused by fact that the concrete strength and stiffness were uncertain.

6. Parametric study

The computer program developed was employed to undertake a parametric study on the performance of slender circular DCFST columns subjected to eccentric loading. The parameters examined included the D_i / D_o ratio, D_o / t_o ratio, D_i / t_i ratio, L / r ratio, e / D_o ratio, and concrete and steel yield strengths. Details on these columns are provided in Table 2 where these columns were grouped into seven groups. All analyses included an initial out-of-straightness of L/1000 at the column mid-height. The Young's modulus of steel was 200 GPa.

6.1. Effects of D_i / D_o ratio

The Group 1 columns shown in Table 2 were used to examine the influences of the D_i / D_o ratio on the axial load-deflection relations of eccentrically loaded DCFST slender columns. The diameter of the internal steel tubes was varied to give D_i / D_o ratios of 0.25, 0.4, 0.55 and 0.7. Fig. 7 presents the computed axial loads of DCFST slender columns as a function of mid-height deflections with D_i / D_o ratios ranging from 0.25 to 0.7. The figure illustrates that the use of a larger D_i / D_o ratio markedly lowers the column initial stiffness and significantly reduces their ultimate axial loads. When the D_i / D_o ratio of 0.25 is changed to 0.4, 0.55 and 0.7, the calculated ultimate axial load of the slender column is reduced by 4.5%, 10.7% and 23.3%, respectively. It is seen from Fig. 7 that the displacement ductility of DCFST slender columns is generally reduced by increasing the D_i / D_o ratio, but the column with D_i / D_o ratio of 0.55 exhibits highest displacement ductility compared with other columns in Group 1.

6.2. Effects of D_o/t_o ratio

Numerical simulations of DCFST slender columns made of concrete with compressive strength of 65 MPa given in Group 2 in Table 2 were performed to quantify the influences of D_o/t_o ratio on their responses of axial load-deflections. The diameter of the external steel tube was changed from 500 to 650 to produce different D_o/t_o ratios of 50, 55, 60 and 65. The predicted axial loads as a function of the mid-height deflections are depicted in Fig. 8. It is seen that the column initial stiffness is remarkably increased by increasing the D_o/t_o ratio in terms of the diameter of the outer steel tube while keeping other parameters unchanged. It is found that the ultimate axial loads of DCFST slender columns are significantly increased by using larger D_o/t_o ratios. The numerical solutions computed demonstrate that the increases in the column ultimate axial strength are 23.5%, 47.9% and 73.7%, respectively by increasing the D_o/t_o ratio from 50 to, 55, 60 and 65. The effects of D_o/t_o ratios on the behavior of CFST columns and DCFST short columns by keeping the D_o unchanged and varying t_o have been investigated by Liang [11, 32].

6.3. Effects of D_i/t_i ratio

The effects of D_i/t_i ratios on the column behavior were examined. The columns shown in Group 3 in Table 2 had the *L*/*r* ratio of 50 and the e/D ratio of 0.2. The thickness of the internal steel tube was varied to obtain the D_i/t_i ratios of 20, 30, 35 and 40 specified in the numerical analyses. The computational responses of the columns with different D_i/t_i ratios in terms of axial loads and deflections are plotted in Fig. 9. The effects of D_i/t_i ratios on the initial stiffness of DCFST slender columns at initial loading stages are very minor. The

ultimate strength of DCFST slender columns under eccentric loads is considerably reduced by increasing the D_i / t_i ratios. It appears from Fig. 9 that the percentage reductions in the ultimate axial loads calculated are 4.3%, 6.0% and 7.2% respectively by changing the D_i / t_i ratio from 20 to 30, 35 and 40.

6.4. Effects of column slenderness ratio

The computer program was employed to analyze DCFST slender columns in Group 4 given in Table 2 to study the influences of column slenderness on their performance. The column slenderness ratios of 40, 60, 80 and 100 were computed by varying the column length while other geometric and material parameters were not changed. The loading eccentric ratio (e / D) was 0.25. The calculated axial load-deflection characteristics of DCFST slender columns with *L*/*r* ratios ranging from 40 to 100 are presented in Fig. 10. It appears that both the column initial stiffness and ultimate load are significantly reduced by increasing the column length. Increasing the *L*/*r* ratio from 40 to 60, 80 and 100 leads to 21.2%, 39.2% and 53% reductions in the column ultimate axial load, respectively. As shown in Fig. 10, increasing the *L*/*r* ratio generally improves the displacement-ductility of slender columns. The investigations show that the influence of the column slenderness on the performance of DCFST column is the most pronounced.

6.5. Effects of eccentricity ratio

The eccentricity of the applied axial load is a key factor that affects the responses of slender DCFST columns. Numerical analyses were performed to study the responses of DCFST slander columns having e / D ratios ranging from 0.1 to 0.4 as shown in Group 5 in Table 2.

The column slenderness ratio was 45. Figure 11 gives the predicted relationships of axial loads, deflections and loading eccentricity ratio. The results demonstrate that the strength and ductility of DCFST slender columns is significantly affected by the eccentricity of the applied loads. The higher the eccentricity ratio, the lower the initial stiffness and ultimate axial strength of the DCFST column. Changing the e / D ratio from 0.1 to 0.2, 0.3 and 0.4 leads to an reduction in the column ultimate axial strength by 13.1%, 23.5% and 32.1%, respectively.

6.6. Effects of concrete compressive strength

In Group 6 shown in Table 2, DCFST slender columns were constructed by concrete of different compressive strengths varying from 40 to 100 MPa. This group of columns where the L/r ratio was 40 and the e / D ratio was 0.3 were analyzed to examine the effects of the concrete strengths on the column behavior. The compressive concrete strengths of 40, 60, 80 and 100 MPa were assigned for the sandwiched concrete in computer analyses, respectively. The deflections of slender DCFST columns subjected to increasing loading are presented in Fig. 12. It is observed that the use of higher concrete strength slightly increases the column initial stiffness. More importantly, increasing the strength of sandwiched concrete results in a significant increase in the column ultimate axial strengths. If the 40 MPa concrete is replaced by 60, 80 and 100 MPa respectively, the column ultimate axial strength will increase by about 20.3%, 39.6% and 59%, respectively.

The influences of concrete strengths on the column strength curves were investigated by varying the column slenderness of the columns given in Group 6. Figure 13 presents the column strength curves varied with concrete strengths predicted by the computer program. The figure demonstrates that the column ultimate axial strength increases with increasing the

concrete strength regardless of the column slenderness. The concrete strength has the most pronounced influence on the axial capacity of cross-sections and this effect decreases when the column slenderness is increased. As demonstrated in Fig. 13, when $L/r = 0$ and increasing $f_c^{'}$ from 40 to 60, 80 and 100 MPa, the column ultimate axial load increases by 20.9%, 41.7% and 62.3%, respectively. In contrast, when $L/r = 120$ and replacing 40 MPa concrete with 60, 80 and 100 MPa concrete respectively, the column ultimate axial strength increases by 10.4%, 18.4% and 25.4%, respectively. However, the column ultimate axial strength with $L/r = 120$ and $f_c^{'} = 100\,\text{MPa}$ is only 40.3% of its cross-sectional capacity with $f_c^{'} = 40\,\text{MPa}$. This suggests that it is more effective to increase the dimension of the cross-section rather than the concrete strength for very slender DCFST columns.

6.7. Effects of steel yield strength

The influences of the yield strengths of steel tubes on the performance of DCFST slender circular columns in Group 7 shown in Table 2 were investigated. These columns were filled with 90 MPa high-strength concrete and their *L*/*r* ratio was 35 and e/D ratio was 0.35. Figure 14 depicts the column axial loads as a function of deflections and steel yield strengths ranging from 250 to 450 MPa. The yield stress does not have an influence on the column initial stiffness but at higher loads, steel tubes with higher yield strengths exhibit higher bending stiffness. The higher the yield strength of the steel tubes, the higher the column ultimate axial strength. If the yield strength of steel tubes is changed from 250 to 300, 350 and 450 MPa, the column axial capacity is expected to be 6.3%, 12.2% and 22.8%, respectively.

6.8. Load distributions in steel tubes and concrete

The computer program developed was used to study the load distributions in the external and internal steel tubes as well as in sandwiched concrete in eccentrically-loaded circular slender DCFST columns. Numerical analyses on DCFST slender columns shown in in Group 4 in Table 2 were carried out to explore the influences of columns slenderness on the load distributions in DCFST columns. The calculated axial load-deflection responses of steel tubes, sandwiched concrete and DCFST slender columns are presented in Fig. 15. It appears that a large portion of the axial load is carried by the sandwiched concrete regardless of the column slenderness. In addition, when the axial load of the DCFST column with $L/r = 40$ falls to 60% of the column ultimate axial load (P_u), all of the concrete and steel components carry compressive axial loads. However, for DCFST columns with $L/r \geq 60$, when the column axial load falls to $0.6P_u$, the outer and inner steel tubes are subjected to tensile resultant forces as shown in Fig. 15. The reason for this is that very slender DCFST columns are subjected to large deflections and bending moment at the column mid-height, which results in tensile resultant force in the steel tubes. The steel and concrete contribution ratios calculated are given in Fig. 16. Increasing the *L*/*r* ratio generally decreases the contribution ratios of the inner steel tube and concrete but increases the contribution ratio of the outer tube. At the ultimate strength limit state, the contribution ratios of concrete, external steel tube and internal steel tube are obtained as 0.639, 0.208 and 0.153, respectively.

Group 5 DCFST columns where the *L*/*r* ratio was 45 given in Table 2 were analyzed to study the influences of e/D ratios on the distributions of loads in DCFST slender columns. The load distributions in concrete and steel components with various e/D ratios are shown in Fig. 17. When the axial load falls to $0.6P_u$, all steel tubes and concrete components are subjected to compressive resultant forces regardless of the e/D ratios. As schematically depicted in Fig. 18, the contribution ratios of the sandwiched-concrete and inner steel tube increase with

increasing the e / D ratio. However, increasing the e / D ratio decreases the contribution ratio of the outer steel tube.

6.9. Effects of concrete confinement

The confinement effects on the deflection responses and column strength curves were investigated by analyzing column C1 given in Table 2. As illustrated in Fig. 19, the confinement effect on the column initial stiffness having an L/r ratio of 35 is minor but is significant on its post-peak axial load-deflection responses. When the confinement is not included in the analysis, the column ultimate axial load is underestimated by 9.8%. The column strength curves of the DCFST columns including or ignoring confinement are demonstrated in Fig. 20. The effect of confinement on the section axial capacity is the most pronounced, generally decreasing with increasing the L/r ratio. When the L/r ratio is 61, the column ultimate axial strength considering confinement increases only by 0.09%. However, when the L/r ratio is greater than 61, however, the column ultimate axial load considering confinement is slightly underestimated. This suggests that the design of very slender DCFST columns may ignore confinement effects.

7. Conclusions

A mathematical model has been presented in this paper for the simulation of the performance of circular DCFST slender columns with high-strength concrete subjected to eccentric loads. The computational algorithms implementing the mathematical model have been developed that calculate the axial load-deflections of circular slender DCFST columns. The accurate constitutive laws of sandwiched concrete with the ability to quantify the post-peak behavior

have been incorporated in the mathematical model and discussed in details. The proposed mathematical model has been verified by the experimental results of DCFST slender columns reported in the published literature. The developed computer program has been utilized to quantify the ultimate axial loads, axial load-deflection responses, column strength curves, load distributions in steel tubes and concrete and confinement characteristics of high-strength DFCST slender columns with a wide range of geometric and material parameters. It has been demonstrated that the mathematical model is an efficient and accurate simulation and design technique for circular slender DCFST columns constructed by high-strength concrete.

Based on the parametric study, the following important conclusions are drawn:

(1) Increasing the D_i / D_o ratio (increasing D_i only) considerably decreases the initial stiffness of a DCFST slender column but significantly reduces its ultimate axial load.

(2) The use of a larger outer steel tube remarkably improves the initial stiffness of the DCFST slender column and significantly increases the column ultimate axial strength.

(3) The D_i / t_i ratio has a minor effect on the column initial stiffness but considerable effect on the ultimate axial strength of a DCFST slender column.

(4) Increasing the *L/r* ratio reduces the initial stiffness and ultimate axial load of a DCFST column, and the contribution ratios of the inner steel tube and concrete, but increases the column displacement ductility and the contribution ratio of the outer steel tube.

(5) Increasing the e / D ratio significantly reduces the ultimate axial strength, initial stiffness, ductility of a CFDST column and the contribution ratio of the outer steel tube, but increases the contribution ratios of the concrete and inner steel tube.

(6) The column ultimate axial strength is significantly increased by using higher strength concrete. The effect of the concrete strength is most pronounced on the section axial strength and this effect is found to decrease with an increase in the column slenderness.

(7) The use of higher strength steel tubes in a CFDST slender columns leads to higher column ultimate axial load.

(8) The confinement effect is the most pronounced on the section ultimate axial strength, but it decreases with increasing the column slenderness ratio. For DCFST columns with $L/r > 61$, the confinement effect can be ignored in the design.

References

[1] Tao Z, Han LH, Zhao XL. Behavior of concrete-filled double skin (CHS inner and CHS outer) steel tubular stub columns and beam-columns. J Constr Steel Res 2004; 60: 1129-1158.

[2] Essopjee Y, Dundu M. Performance of concrete-filed double-skin circular tubes in compression. Compos Struct, 2015; 133:1276-1283.

[3] Ibañez C, Romero ML, Espinos, A, Portolés JM, Albero V. Ultra-high strength concrete on eccentrically loaded slender circular concrete-filled dual steel columns. Structures 2017; 12: 64-74.

[4] Knowles RB, Park R. Strength of concrete-filled steel tubular columns. J Struct Div, ASCE 1969; 95(12):2565-2587.

[5] Neogi, PK, Sen HK, Chapman JC. Concrete-filled tubular steel columns under eccentric loading. Struct Eng 1969; 47(5): 187-195.

[6] Rangan B, Joyce M. Strength of eccentrically loaded slender steel tubular columns filled with high-strength concrete. ACI Struct J 1992; 89(6): 676-681.

[7] Schneider SP. Axially loaded concrete-filled steel tubes. J Struct Eng, ASCE 1998; 124(10):1125-1138.

[8] Giakoumelis, G, Lam D. Axial load capacity of circular concrete-filled tube columns. J Constr Steel Res 2004; 60: 1049-1068.

[9] Portolés JM, Romero, ML, Bonet JL, Filippou FC. Experimental study of high strength concrete-filled circular tubular columns under eccentric loading. J Constr Steel Res 2011; 67(4): 623-633.

[10] Liang QQ. High strength circular concrete-filled steel tubular slender beam-columns, Part I: Numerical analysis. J Constr Steel Res 2011; 67(2): 164-171.

[11] Liang QQ. High strength circular concrete-filled steel tubular slender beam-columns, Part II: Fundamental behavior. J Constr Steel Res 2011; 67(2): 172-180.

[12] Wei S, Mau ST, Vipulanandan C, Mantrala SK. Performance of new sandwich tube under axial loading: Experiment. J Struct Eng, ASCE 1995; 121(12): 1806-1814.

[13] Zhao XL, Grzebieta R, Elchalakan M. Tests of concrete-filled double skin CHS composite stub columns. Steel Compos Struct 2002; 2(2): 129-146.

[14] Han LH, Huang H, Tao Z, Zhao XL. Concrete-filled double skin steel tubular (CFDST) beam–columns subjected to cyclic bending**.** Eng Struct 2006; 28(12):1698-1714.

[15] Uenaka K, Kitoh H, Sonoda K. Concrete filled double skin circular stub columns under compression. Thin-Walled Struct 2010; 48: 19-24.

[16] Hajjar JF, Schiller PH, Molodan A. A distributed plasticity model for concrete-filled steel tube beam-columns with interlayer slip. Eng Struct 1998;20(8):663-676.

[17] Susantha KAS, Ge HB, Usami T. Uniaxial stress-strain relationship of concrete confined by various shaped steel tubes. Eng Struct 2001;23(10):1331-1347.

[18] Shanmugam NE, Lakshmi B, Uy B. An analytical model for thin-walled steel box columns with concrete in-fill. Eng Struct 2002;24(6):825-838.

[19] Hu, HT, Huang CS, Wu MH, Wu YM. Nonlinear analysis of axially loaded concrete-filled tube columns with confinement effect. J Struct Eng, ASCE 2003; 129(10): 1322-1329.

[20] Hatzigeorgiou GD. Numerical model for the behavior and capacity of circular CFT columns, Part I: Theory. Eng Struct 2008; 30(6): 1573-1578.

[21] Liang QQ, Fragomeni S. Nonlinear analysis of circular concrete-filled steel tubular short columns under axial loading. J Constr Steel Res 2009; 65(12): 2186-2196.

[22] Portolés JM, Romero ML, Filippou FC, Bonet JL. Simulation and design recommendations of eccentrically loaded slender concrete-filled tubular columns. Eng Struct 2011; 33(5): 1576-1593.

[23] Mollazadeh MH, Wang YC. New insights into the mechanism of load introduction into concrete-filled steel tubular column through shear connection. Eng Struct 2014;75 :139–151.

[24] Kostic SM, Filippou FC, Deretic-Stojanovic B. Generalized plasticity model for inelastic RCFT column response. Comput Struct 2016; 168: 56-67.

[25] Yang YF, Han LH. Concrete filled steel tube (CFST) columns subjected to concentrically partial compression. Thin-Walled Structures 2012; 50(1): 147-156.

[26] Schnabl S, Jelenić G, Planinc I. Analytical buckling of slender circular concrete-filled steel tubular columns with compliant interfaces. Journal of Constructional Steel Research 2015; 115: 252-262.

[27] Wei S, Mau ST, Vipulanandan C, Mantrala SK. Performance of new sandwich tube under axial loading: Analysis. J Struct Eng, ASCE 1995; 121(12): 1815-1821.

[28] Huang H, Han LH, Tao Z, Zhao XL. Analytical behavior of concrete-filled double skin steel tubular (CFDST) stub columns. J Constr Steel Res 2010; 66: 542-555.

[29] Hu HT, Su FC. Nonlinear analysis of short concrete-filled double skin tube columns subjected to axial compressive forces. Mar Struct 2011; 24: 319-337.

[30] Pagoulatou M, Sheehan T, Dai XH, Lam D. Finite element analysis on the capacity of circular concrete-filled double-skin steel tubular (CFDST) stub columns. Eng Struct 2014; 72: 102-112.

[31] Hassanein MF, Kharoob OF, Liang QQ. Circular concrete-filled double skin tubular short columns with external stainless steel tubes under axial compression. Thin-Walled Structures 2013; 73:252-263.

[32] Liang QQ. Nonlinear analysis of circular double-skin concrete-filled steel tubular columns under axial compression. Eng Struct 2017; 131: 639-650.

[33] Hassanein MF, Kharoob OF. Analysis of circular concrete-filled double skin tubular slender columns with external stainless steel tubes. Thin-Walled Structures 2014; 79: 23-37.

[34] Quach WM, Teng JG, Chung KF. Three-stage full-range stress-strain model for stainless steels. J Struct Eng ASCE 2008; 134(9): 1518-1527.

[35] Ky VS, Tangaramvong S, Thepchatri T. Inelastic analysis for the post-collapse behavior of concrete encased steel composite columns under axial compression. Steel Compos Struct 2015;19(5):1237-58.

[36] Liang QQ. Performance-based analysis of concrete-filled steel tubular beam-columns. Part I: Theory and algorithms. J Constr Steel Res 2009; 65(2): 363-373.

[37] Liang QQ. Performance-based analysis of concrete-filled steel tubular beam-columns. Part II: Verification and applications. J Constr Steel Res 2009; 65(2): 351-362.

[38] Liang QQ. Analysis and design of steel and composite structures. Boca Raton and London: CRC Press, Taylor and Francis Group; 2014.

[39] Patel VI, Liang QQ, Hadi, MNS. Nonlinear analysis of concrete-filled steel tubular columns. Scholar's Press: Germany; 2015.

[40] Müller DE. A method for solving algebraic equations using an automatic computer. MTAC 1956; 10:208-215.

[41] Patel VI, Liang QQ, Hadi MNS. High strength thin-walled rectangular concrete-filled steel tubular slender beam-columns. Part I: Modeling. J Constr Steel Res 2012;70:377-384.

[42] Liang QQ, Patel VI, Hadi MNS. Biaxially loaded high-strength concrete-filled steel tubular slender beam-columns. Part I: Multiscale simulation. J Constr Steel Res 2012;75:64-71.

[43] Richart FE, Brandtzaeg A, Brown RL. A study of the failure of concrete under combined compressive stresses. Bull. 185, University of Illionis, Engineering experimental Station, Champaign, III, 1928.

[44] Mander JB, Priestly MNJ, Park R. Theoretical stress-strain model for confined concrete. J Struct Eng, ASCE 1988; 114(8):1804-1826.

[45] ACI Committee 363. State of the Art Report on High-Strength Concrete, ACI Publication 363R-92, Detroit, MI: American Concrete Institute, 1992.

Liang, Q. Q. (2018). Numerical simulation of high strength circular double-skin concrete-filled steel tubular slender columns. *Engineering Structures*, 168: 205-217.

Figures and Tables

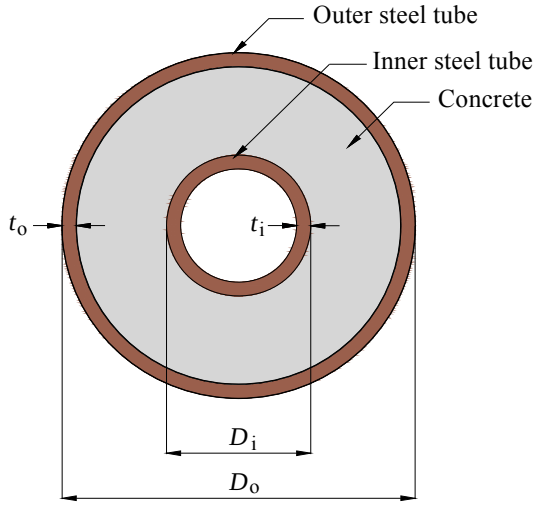

Fig. 1. Cross-section of circular DCFST column

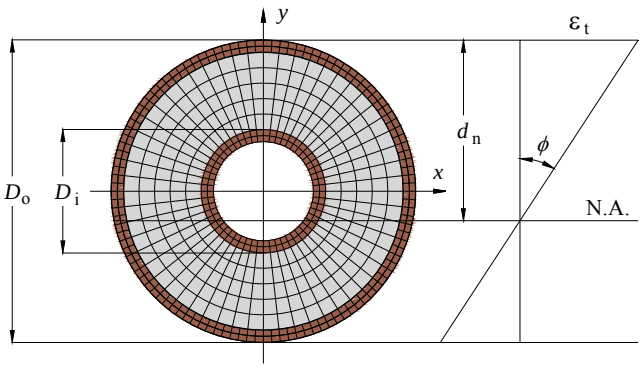

Fig.2. Fibers and strain distribution in circular DCFST column section.

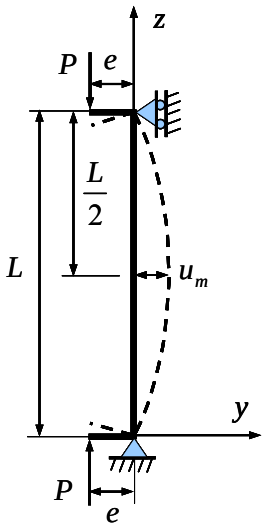

Fig. 3. Pin-ended DCFST slender column under eccentric loading

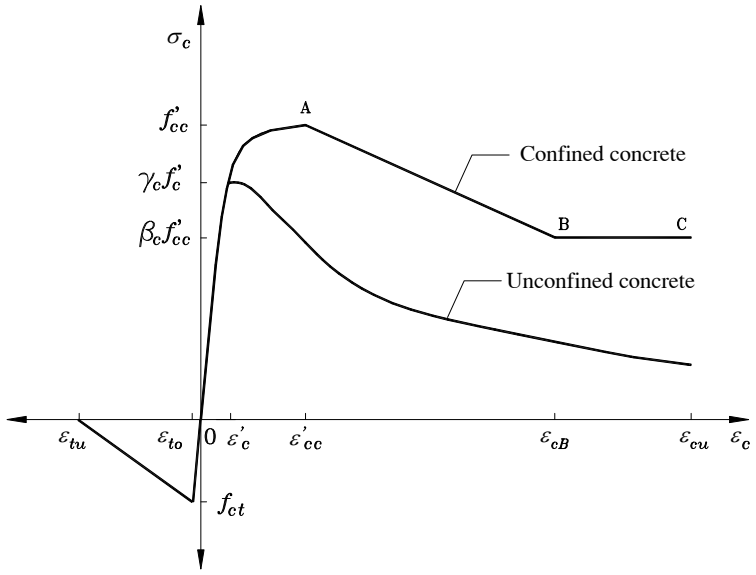

Fig. 4. General stress-strain curve for confined concrete in DCFST columns

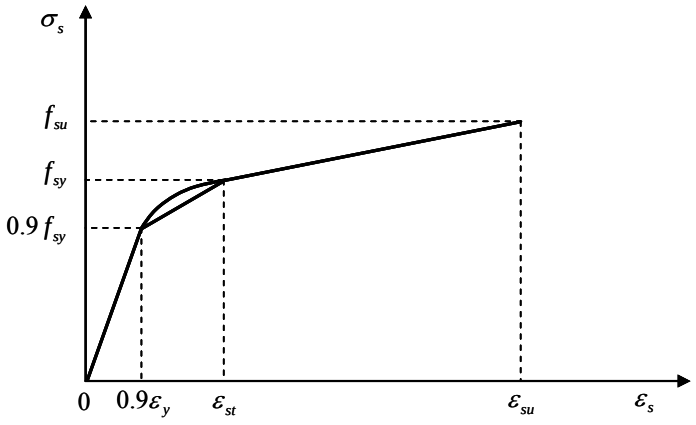

Fig. 5. Stress-strain curve for structural steels

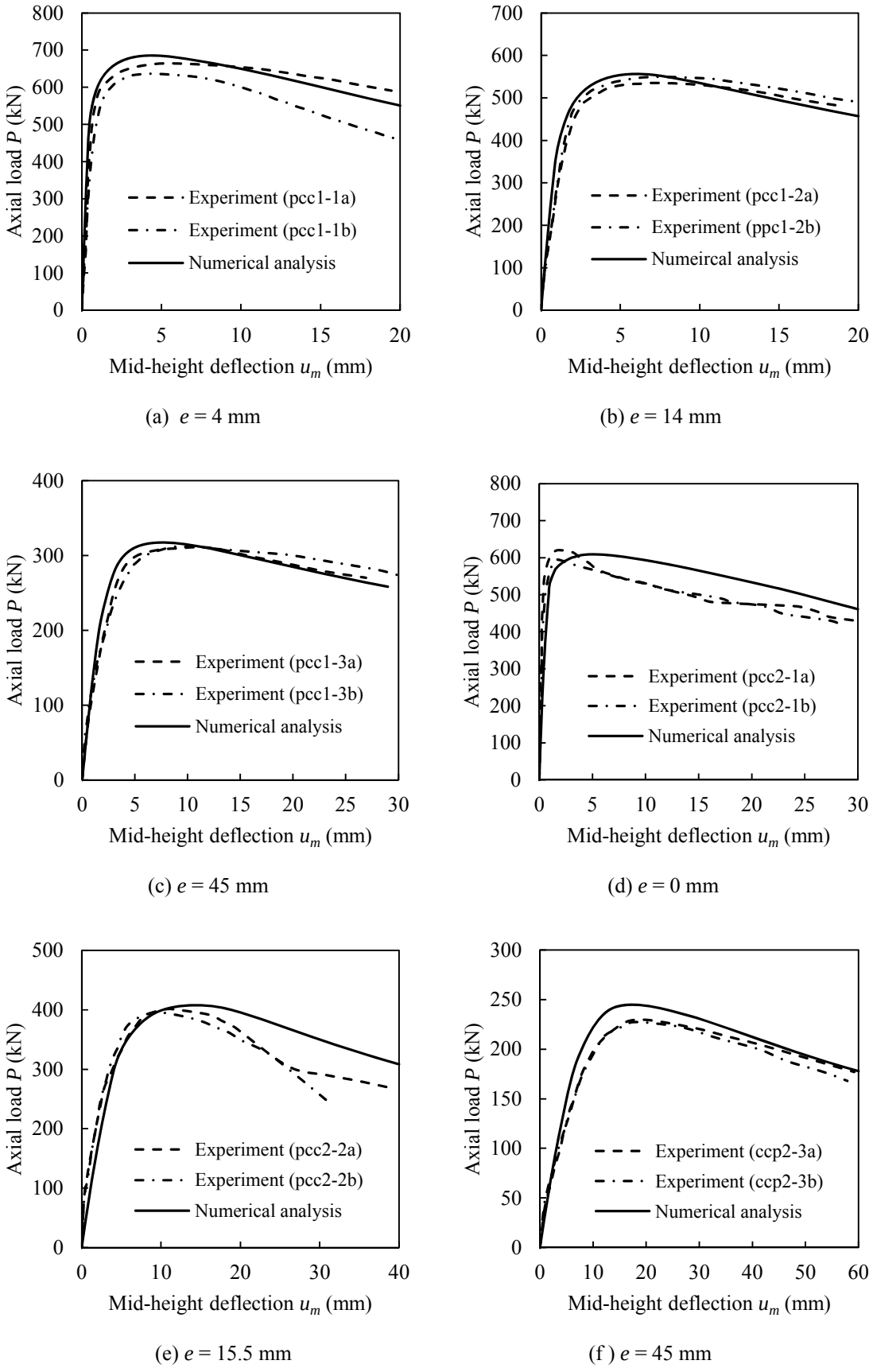

Fig. 6. Comparison of predicted and experimental axial load-deflection curves.

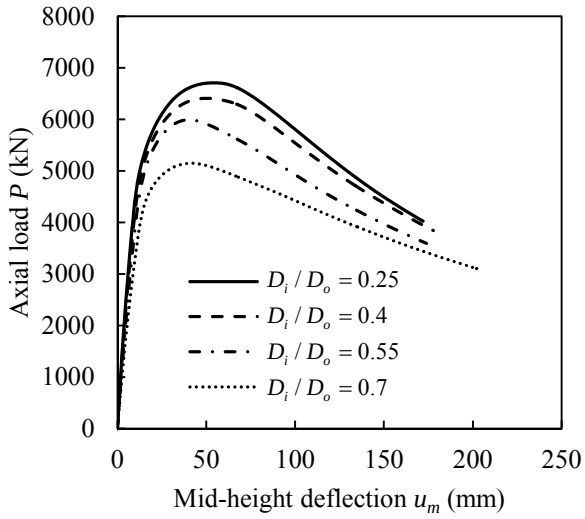

Fig. 7. Axial load-deflection responses of circular DCFST slender columns with various D_i / D_o ratios

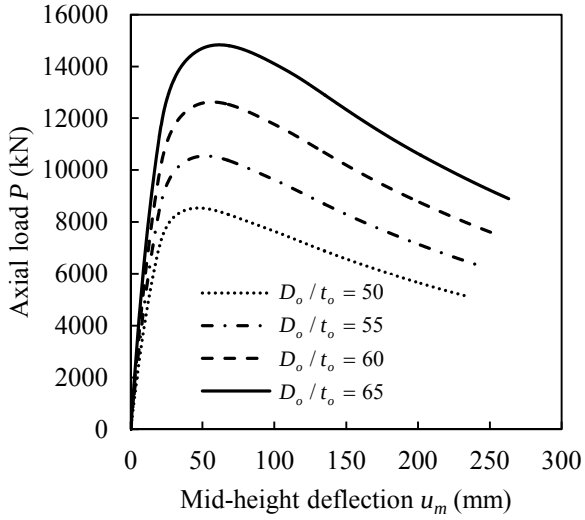

Fig. 8. Axial load-deflection responses of circular DCFST slender columns with various D_o / t_o ratios

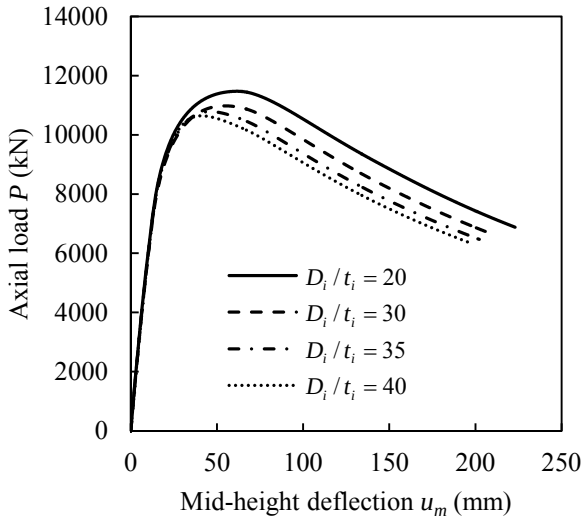

Fig. 9. Axial load-deflection responses of circular DCFST slender columns with various D_i / t_i ratios

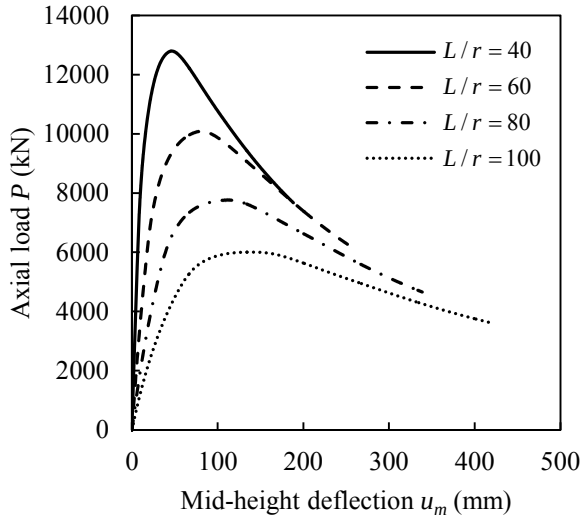

Fig. 10. Axial load-deflection responses of circular DCFST slender columns with various L / r ratios

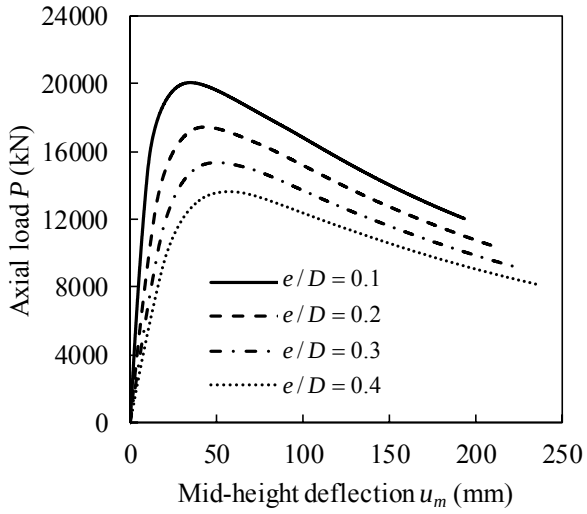

Fig. 11. Axial load-deflection responses of circular DCFST slender columns with various e/D ratios.

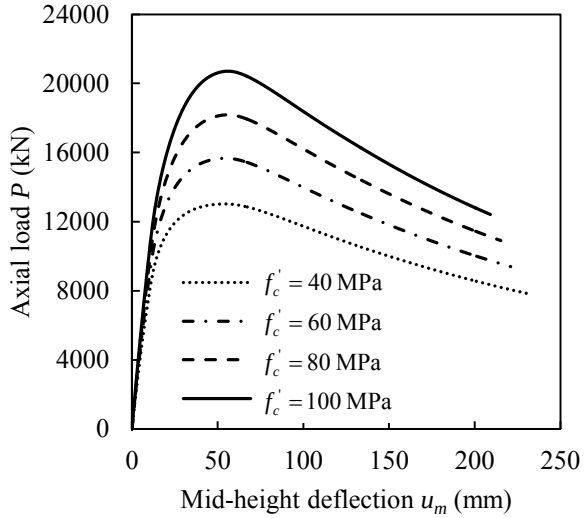

Fig. 12. Axial load-deflection responses of circular DCFST slender columns with various concrete compressive strengths

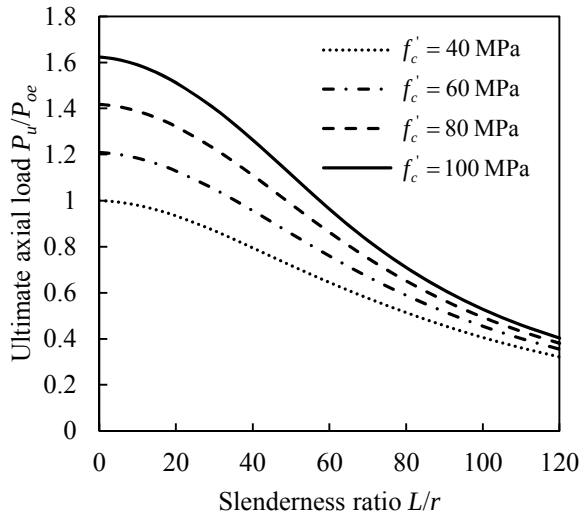

Fig. 13. Effects of concrete compressive strengths on the column strength curves

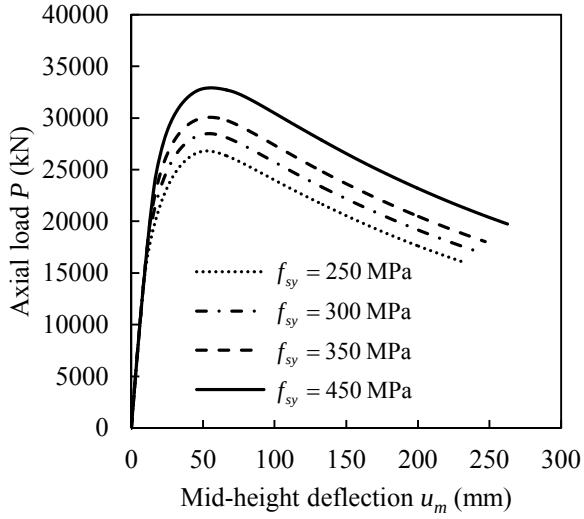

Fig. 14. Axial load-deflection responses of circular DCFST slender columns with various steel yield strengths

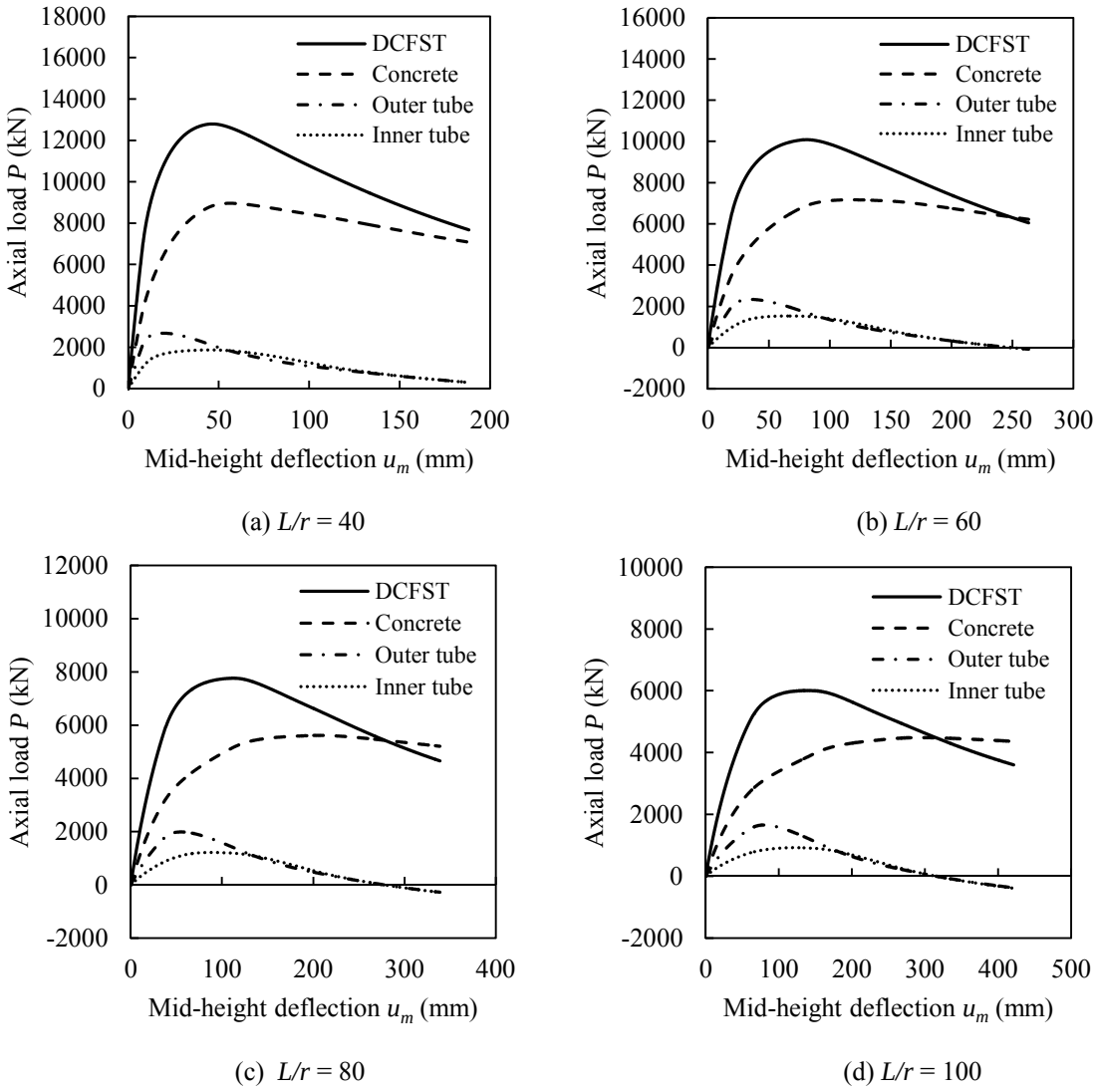

Fig. 15. Load distributions in circular DCFST slender columns with various L/r ratios

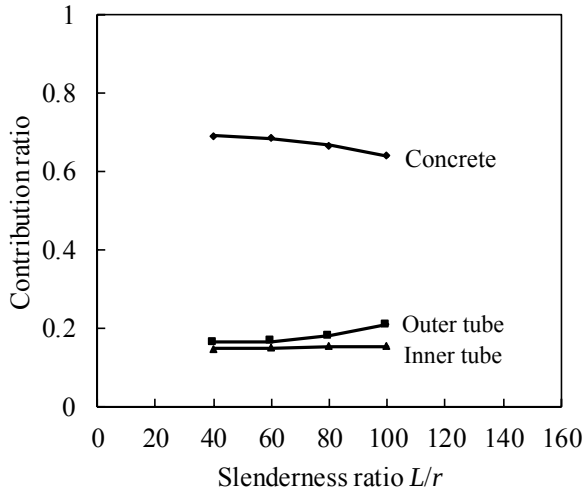

Fig. 16. Steel and concrete contribution ratios as a function of L/r ratio.

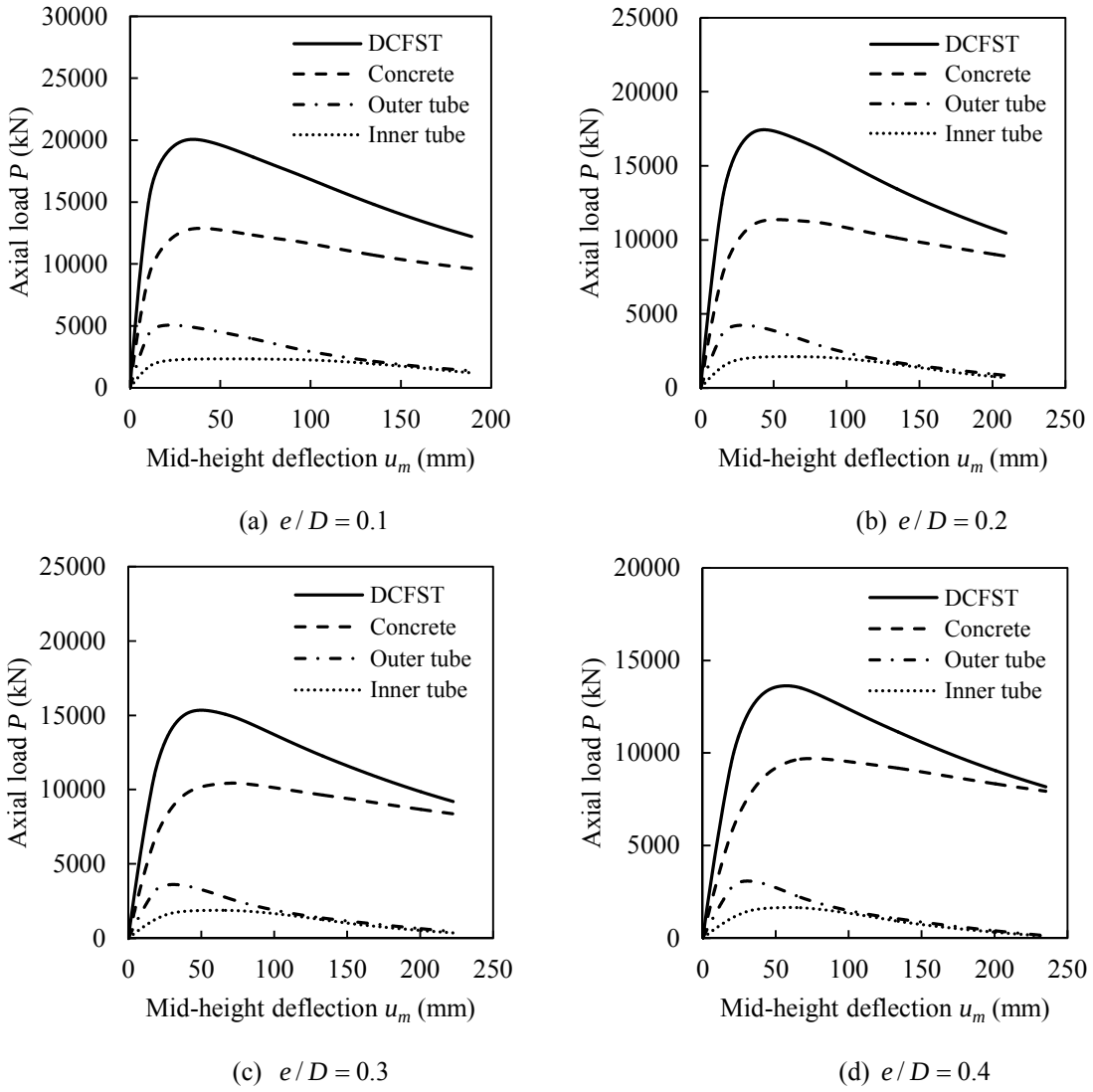

Fig. 17. Load distributions in circular DCFST slender columns with various e/D ratios.

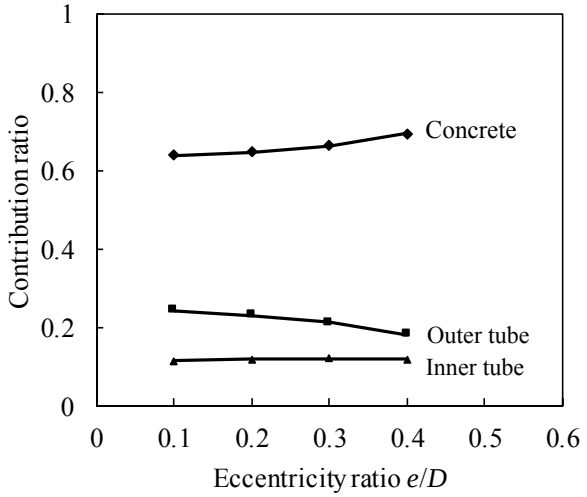

Fig. 18. Steel and concrete contribution ratios as a function of e/D ratio.

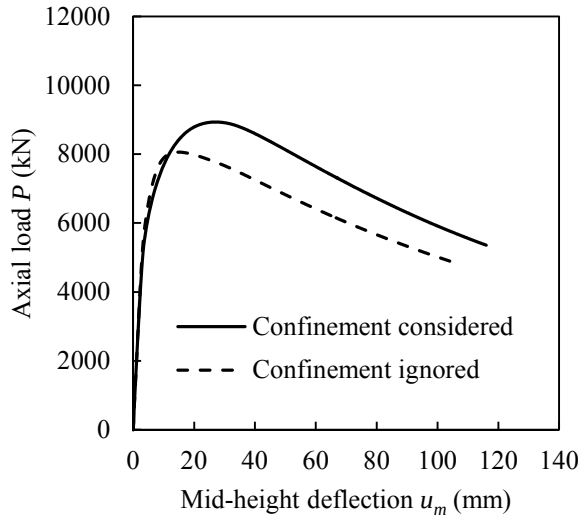

Fig. 19. Effects of concrete confinement on the axial load-deflection responses of circular DCFST columns

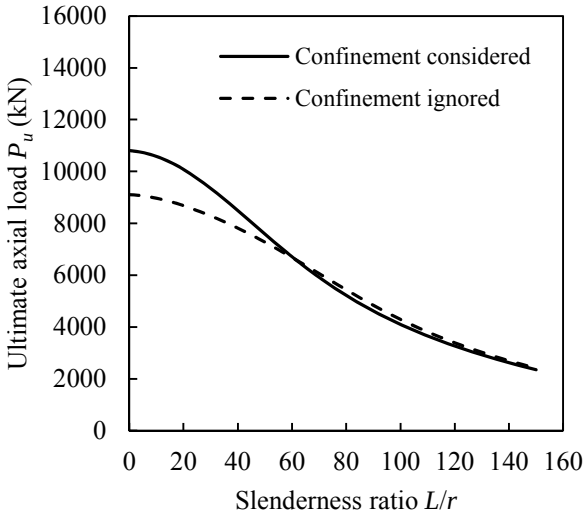

Fig. 20. Effects of concrete confinement on the column strength curve of circular DCFST columns

Liang, Q. Q. (2018). Numerical simulation of high strength circular double-skin concrete-filled steel tubular slender columns. *Engineering Structures*, 168: 205-217.

Table 1. Ultimate axial strengths of circular DCFST slender columns

Specimen	$D_o \times t_o$ (mm)	$D_i \times t_i$ (mm)	L (mm)	e (mm)	f_{syo} (MPa)	f_{syi} (MPa)	f_c' (MPa)	$P_{u.\exp}$ (kN)	$P_{u.\mathrm{num}}$ (kN)	$\frac{P_{u.\mathrm{num}}}{P_{u.\exp}}$	Ref.
pcc1-1a	114×3	58×3	887	4	294.5	374.5	39.3	664	685.6	1.033	[1]
pcc1-1b	114×3	58×3	887	4	294.5	374.5	39.3	638	685.6	1.075	
Pcc1-2a	114×3	58×3	887	14	294.5	374.5	39.3	536	556.5	1.038	
pcc1-2b	114×3	58×3	887	14	294.5	374.5	39.3	549	556.5	1.014	
pcc1-3a	114×3	58×3	887	45	294.5	374.5	39.3	312	317.3	1.017	
pcc1-3b	114×3	58×3	887	45	294.5	374.5	39.3	312	317.3	1.017	
pcc2-1a	114×3	58×3	1770	0	294.5	374.5	39.3	620	609.2	0.983	
pcc2-1b	114×3	58×3	1770	0	294.5	374.5	39.3	595	609.2	1.024	
pcc2-2a	114×3	58×3	1770	15.5	294.5	374.5	39.3	400	407.6	1.019	
pcc2-2b	114×3	58×3	1770	15.5	294.5	374.5	39.3	394	407.6	1.035	
pcc2-3a	114×3	58×3	1770	45	294.5	374.5	39.3	228	244.9	1.074	
pcc2-3b	114×3	58×3	1770	45	294.5	374.5	39.3	227	244.9	1.079	
S139.2-1.0a	139.2×3	76×2	998	0	418	324	26.2	1059.2	1041.2	0.983	[2]
S139.2-1.0b	139.2×3	76×2	1001	0	418	324	26.2	1056.1	1040.9	0.986	
S139.2-1.5a	139.2×3	76×2	1500	0	418	324	26.2	905.5	849.8	0.938	
S139.2-1.5b	139.2×3	76×2	1503	0	418	324	26.2	901.6	849.6	0.942	
S139.2-2.0a	139.2×3	76×2	2000	0	418	324	26.2	831.7	805.2	0.968	
S139.2-2.0b	139.2×3	76×2	1998	0	418	324	26.2	837.4	805.5	0.962	
S139.2-2.5a	139.2×3	76×2	2502	0	418	324	26.2	732.1	737.1	1.007	
S139.2-2.5b	139.2×3	76×2	2498	0	418	324	26.2	729	737.7	1.012	
S152.4-1.0a	152.4×3	76×2	1003	0	549	324	26.2	1263.5	1381.8	1.094	
S152.4-1.0b	152.4×3	76×2	1002	0	549	324	26.2	1254.9	1381.9	1.100	
S152.4-1.5a	152.4×3	76×2	1497	0	549	324	26.2	1195.6	1109.5	0.928	
S152.4-1.5b	152.4×3	76×2	1503	0	549	324	26.2	1191.2	1109.1	0.931	
S152.4-2.0a	152.4×3	76×2	1997	0	549	324	26.2	1047.3	1054.8	1.007	
S152.4-2.0b	152.4×3	76×2	2000	0	549	324	26.2	1041.6	1054.3	1.012	
S152.4-2.5a	152.4×3	76×2	2498	0	549	324	26.2	941.4	962.1	1.022	
S152.4-2.5b	152.4×3	76×2	2500	0	549	324	26.2	949	961.7	1.013	
S165.1-1.0a	165.1×3	76×2	998	0	516	324	26.2	1512.3	1529.3	1.011	
S165.1-1.0b	165.1×3	76×2	999	0	516	324	26.2	1510.6	1529	1.012	
S165.1-1.5a	165.1×3	76×2	1504	0	516	324	26.2	1286.4	1210	0.941	
S165.1-1.5b	165.1×3	76×2	1498	0	516	324	26.2	1275.1	1210.4	0.949	
S165.1-2.0a	165.1×3	76×2	2003	0	516	324	26.2	1187.2	1164.9	0.981	
S165.1-2.0b	165.1×3	76×2	1998	0	516	324	26.2	1199.8	1165.5	0.971	
S165.1-2.5a	165.1×3	76×2	2498	0	516	324	26.2	1028	1090.1	1.060	
S165.1-2.5b	165.1×3	76×2	2502	0	516	324	26.2	1036.5	1089.4	1.051	
S193.7-1.0a	193.7×3.5	76×2	1003	0	391	324	26.2	2010	1834.6	0.913	
S193.7-1.0b	193.7×3.5	76×2	1000	0	391	324	26.2	2030	1834.8	0.904	
S193.7-1.5a	193.7×3.5	76×2	1502	0	391	324	26.2	1730	1750.5	1.012	
S193.7-1.5b	193.7×3.5	76×2	1500	0	391	324	26.2	1720	1750.8	1.018	
S193.7-2.0a	193.7×3.5	76×2	1998	0	391	324	26.2	1581.6	1444.4	0.913	
S193.7-2.0b	193.7×3.5	76×2	2003	0	391	324	26.2	1584.1	1444	0.912	
S193.7-2.5a	193.7×3.5	76×2	2503	0	391	324	26.2	1451.4	1395.7	0.962	
S193.7-2.5b	193.7×3.5	76×2	2497	0	391	324	26.2	1458.7	1396.3	0.957	
Mean										0.997	
Standard deviation (SD)										0.051	
Coefficient of variation (COV)										0.051	

Table 2. Geometric and material properties of circular DCFST slender columns used in the parametric study

Group	Column	$D_o \times t_o$ (mm)	D_o / t_o	$D_i \times t_i$ (mm)	D_i / t_i	L / r	e / D (D = 306 mm)	f_c' (MPa)	f_{syo} , f_{syi} (MPa)	f_{suo} , f_{sui} (MPa)
1	C1	450×8	56.25	112.5×6	18.75	60	0.1	60	250	320
	C2	450×8	56.25	180×6	30	60	0.1	60	250	320
	C3	450×8	56.25	247.5×6	41.25	60	0.1	60	250	320
	C4	450×8	56.25	315×6	52.5	60	0.1	60	250	320
2	C5	500×10	50	350×10	35	55	0.15	65	350	430
	C6	550×10	55	350×10	35	55	0.15	65	350	430
	C7	600×10	60	350×10	35	55	0.15	65	350	430
	C8	650×10	65	350×10	35	55	0.15	65	350	430
3	C9	550×11	50	250×12.5	20	50	0.2	70	300	430
	C10	550×11	50	250×8.33	30	50	0.2	70	300	430
	C11	550×11	50	250×7.14	35	50	0.2	70	300	430
	C12	550×11	50	250×6.25	40	50	0.2	70	300	430
4	C13	600×10	60	300×10	30	40	0.25	75	250	320
	C14	600×10	60	300×10	30	60	0.25	75	250	320
	C15	600×10	60	300×10	30	80	0.25	75	250	320
	C16	600×10	60	300×10	30	100	0.25	75	250	320
5	C17	650×10	65	320×8	40	45	0.1	85	350	430
	C18	650×10	65	320×8	40	45	0.2	85	350	430
	C19	650×10	65	320×8	40	45	0.3	85	350	430
	C20	650×10	65	320×8	40	45	0.4	85	350	430
6	C21	700×10	70	330×10	33	40	0.3	40	300	430
	C22	700×10	70	330×10	33	40	0.3	60	300	430
	C23	700×10	70	330×10	33	40	0.3	80	300	430
	C24	700×10	70	330×10	33	40	0.3	100	300	430
7	C25	800×15	53.33	380×15	25.33	35	0.35	90	250	320
	C26	800×15	53.33	380×15	25.33	35	0.35	90	300	430
	C27	800×15	53.33	380×15	25.33	35	0.35	90	350	430
	C28	800×15	53.33	380×15	25.33	35	0.35	90	450	520